ЖЭТФ, 2014, том 145, вып. 3, стр. 525–534 

# EDGE STATES AND TOPOLOGICAL PROPERTIES OF ELECTRONS ON THE BISMUTH ON SILICON SURFACE WITH GIANT SPIN–ORBIT COUPLING

***D. V. Khomitsky**, *A. A. Chubanov***

*University of Nizhny Novgorod*
*603950, Nizhny Novgorod, Russia*

Received August 22, 2013

We derive a model of localized edge states in a finite-width strip for the two-dimensional electron gas formed in the hybrid system of a bismuth monolayer deposited on the silicon interface and described by the nearly free electron model with giant spin-orbit splitting. The edge states have the energy dispersion in the bulk energy gap with a Dirac-like linear dependence on the quasimomentum and the spin polarization coupled to the direction of propagation, demonstrating the properties of a topological insulator. The topological stability of edge states is confirmed by the calculations of the $Z_2$ invariant taken from the structure of the Pfaffian for the time reversal operator for the filled bulk bands in the surface Brillouin zone, which is shown to have a stable number of zeros with the variations of material parameters. The proposed properties of the edge states may support future advances in experimental and technological applications of this new material in nanoelectronics and spintronics.

**DOI**: 10.7868/S0044451014030148

## 1. INTRODUCTION

During the last decade, an increasing attention is given to a new class of structures called topological insulators (TIs) with promising characteristics as regards both fundamental aspects of their physics and possible applications in nanoelectronics, spintronics, and fabrication of new magnetic, optical, and information processing devices [1–5]. The principal features of TIs include the presence of time-reversal invariance in the system where the propagating edge states may exist, being localized near the boundary of the host material and having the dispersion relation that is linear near the origin of their quasimomentum (Dirac-like structure), corresponding to energies belonging to the insulating gap of the bulk material. The spin of such states is firmly attached to the direction of propagation along the edge, making them protected against backscattering due to the time-reversal invariance, which leads to effective cancelation of two scattered states with opposite possible directions of the spin flip that accompanies such backscattering. The existence of such edge states has been shown in numerous theoretical models of TIs, and also in the experiments. The materials included graphene [6], HgTe/CdTe quantum wells [7–10], bismuth thin films [11], quantum wires [12], nanocontacts or bilayers [13], the LiAuSe and KHgSb compounds [14], and general two-dimensional (2D) models of paramagnetic semiconductors [15], silicene [16, 17], and topological nodal semimetals [18]. Another 2D TI has been predicted in the inverted type-II semiconductor InAs/GaSb quantum well [19] and observed experimentally in the contribution of edge modes to the electron transport [20]. Many studies have also been devoted to the general properties of 2D and 3D models of TIs with certain symmetries [17, 21–27], where four topological invariants have been found in 3D TIs instead of a single $Z_2$ invariant in 2D TIs [1, 2, 22].

Recently a general group-theory analysis has been made for the links between the geometry of the Bravais lattice and the properties of TIs [28]. We note that the symmetry arguments always played a significant role in classifying the systems as trivial or topologically protected against external perturbations [6, 21, 28–31]. The time-reversal property of spin-1/2 particles in such systems can be described by the presence of time-reversal invariance (without magnetic impurities or an external magnetic field) and the absence of the spin rotation invariance. Here, the time-reversal operator is given by

*E-mail: khomitsky@phys.unn.ru

$\Theta = i\sigma_y K$, where $K$ is the complex conjugation operator and $\sigma_y$ is the second Pauli matrix. According to the general symmetry considerations [30, 31], this means the class-AII symmetry for the Hamiltonian for which the so-called $Z_2$ topological order is possible for 2D and 3D systems, forming the basis for the TI properties.

The studies of 3D materials were mostly focused on $Bi_2Se_3$, $Bi_2Te_3$, or $Bi_2Te_2Se$ [1, 2, 32–34], where also the edge states were constructed explicitly in several models of finite-size geometry [35, 36]. Another important issue is the effect of impurities and disorder on the band structure and topological stability in TIs. It is known that TIs are robust against weak disorder or the potentials produced by nonmagnetic impurities [6, 21, 37], while the presence of magnetic impurities may lead to hybridization of the insulator atomic orbitals and magnetic material orbitals, producing a strong modification to the metallic or nonmetallic nature of the states and their spin polarization [38]. Even for nonmagnetic impurities, it has been shown recently that the formation of impurity bands within the energy gap at strong doping of the bulk material may lead to their mixing with the edge states of a TI, modifying their structure, although preserving the $Z_2$ order and topological stability [39].

It can be seen that although the features of TIs are very general and describe a truly novel state of matter, the number of different materials demonstrating these features is currently quite limited. It is therefore of interest to find new materials and compounds where possible manifestations of TIs may be present, for both fundamental aspects and applied purposes. It is also necessary to understand which properties of edge states are common for different systems, and which are special, and how all of them are related to the bulk quantum states in a specific model.

Here, we consider a model of edge states and relate their properties to topological characteristics of the host material for a new candidate to the class of TIs: the 2D electron gas in a material with strong spin–orbit coupling (SOC) formed at the interface of a monolayer of bismuth deposited on silicon. This material is characterized by a giant SOC splitting which, was also predicted or observed experimentally in a number of metal films or the combined materials of the "metal on semiconductor" type [40–46], and recently described theoretically [46, 47]. Its huge spin splitting together with the hexagonal type of the lattice creates a certain potential of manifestation of TI properties, since the spin-resolved bands may evolve into spin-resolved edge states, and the hexagonal type of the lattice is favorable for the TI to exist [28].

The properties of the 2D electron gas at the Bi/Si interface have been studied experimentally with the help of angle-resolved photoemission spectroscopy (ARPES) [40–44, 46, 48–50], applied also to other materials. It was found that this material represents an example of the currently widely studied class of materials with a large (up to 0.2–0.4 eV) SOC spin splitting of their energy bands, which can be formed in various compound materials or heterostructures of the "metal on semiconductor" type. It has been known for many years that SOC plays an important role in the formation of TI properties [51], including the localization effects of the Rashba SOC combined with electron–electron interaction [52], the Dirac-cone surface states in $Bi_2Se_3$ [53] and $Bi_2Te_xSe_{3-x}$ [54], $PbSb_2Te_4$ or $Pb_2Bi_2Te_2S_3$ [55], and $Bi_{1-x}Sb_x$ [56], topological phases [57, 58] and the quantum spin Hall phase in a honeycomb lattice [59], the ultracold Fermi gases [60], the spin Hall effect in graphene [61], and the Kondo insulator effects [62, 63].

Various materials with a strong SOC have been the subject of intensive recent studies, including the structures of Bi deposited on Si–Ge substrates [64], the Pb on Si structure [43], the trilayer Bi–Ag–Si system [42], the structures with a monolayer of Pb atoms covering the Ge surface [65] or the Pb on Ge structures [66]. We also mention new types of triple bulk compounds with strong SOC like $GeBi_2Te_4$ [67], BiTeI, or other bismuth tellurohalides [68–70] or the recently discussed $Bi_{14}Rh_3I_9$ material [71].

In this paper, we adopt the nearly free model of two-dimensional bulk states in Bi/Si, developed earlier [46] and applied in the extended form in our previous paper for the description of spin polarization, charge conductance, and optical properties of this promising material [47], for the calculation of 1D edge states of electrons on the Bi/Si interface in a finite strip geometry. We obtain both the explicit form of edge wavefunctions and the edge energy spectrum, calculate their spin polarization, and relate the possible topological stability of their properties to the $Z_2$ topological invariant studied by analyzing the behavior of the matrix elements of the time-reversal operator in the Brillouin zone [1, 2, 5, 6, 21, 23]. The results of our paper are of interest for expanding the knowledge of new materials with the topologically protected properties where the SOC plays a significant role, making them suitable for further applications in spintronics as stable current-carrying and spin-carrying channels.

The paper is organized as following. In Sec. 2, we briefly describe the nearly free electron (NFE) model of 2D bulk states at a Bi/Si interface, and derive a

model for 1D edge states for the electrons in a finite strip geometry. We calculate their spectrum, wavefunctions, and spin polarization. In Sec. 3, we reinforce our findings on the edge state stability by considering the topological band properties of 2D bulk states in Bi/Si, and find the results supporting the presence of the TI phase. Our conclusions are given is Sec. 4.

## 2. MODEL FOR BULK STATES AND EDGE STATES

### 2.1. Bulk states

Our model for 1D edge states is based on the 2D NFE model for bulk states of the 2D electron gas formed at the interface of the trimer Bi/Si(111) structure [46] developed for the description of the spectrum near the $M$ point of the Brillouin zone (BZ), and later extended to modeling the electron states in the entire BZ [47]. This model was compared with its expansion containing anisotropic terms in the NFE model as well as with an empirical tight-binding model [46]. While the details of band structure and the quality of reproducing the experimental ARPES data on energy bands in Bi/Si vary from model to model, the simple NFE model allows reconstructing the main properties of spin-split bands including the magnitude of splitting, the energy gap, and the spin polarization. It also has a major advantage of a straightforward derivation of edge states in a finite-strip geometry, as we see below.

In this model, the Hamiltonian of the 2D electron gas in the BZ of the $(k_x, k_y)$ plane, $H = H_0 + V(x, y)$, is written as a sum of a free-electron term with SOC,

$$H_0 = \frac{\hbar^2 k^2}{2m} + \alpha_R(\sigma_x k_y - \sigma_y k_x), \tag{1}$$

$k^2 = k_x^2 + k_y^2$, corresponding to the Rashba paraboloid centered at the $\Gamma$ point of the hexagonal BZ, and the lattice potential represented via the spatial Fourier expansion with reciprocal space vectors $\mathbf{G}_i$:

$$V(x, y) = \sum_i V_i \exp(i\mathbf{G}_i \cdot \mathbf{r}). \tag{2}$$

The parameters of both $H_0$ and $V$ are fitted so as to provide the best correspondence between the model and the structure of bands near the Fermi level experimentally known from ARPES measurements [42–44, 46]. The typical values [46, 47] are $m = 0.8m_0$, $\alpha_R = 1.1$ eV $\cdot$ Å, and $V_i = V_0 = 0.3$ eV, although they should be treated as fitting parameters rather than measured material constants, and we here consider their variations in the range 0.3–0.6 eV for $V_0$ and

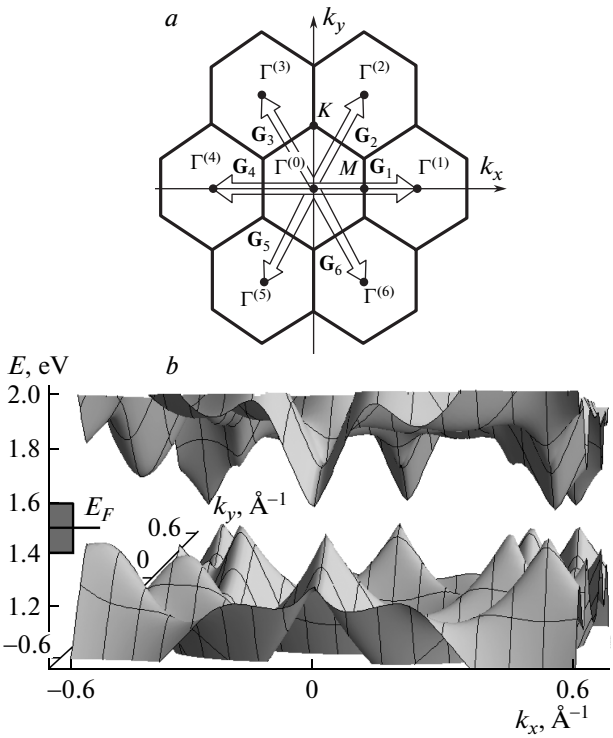


**Fig. 1.** ($a$) The structure of reciprocal space vectors connecting the equivalent $\Gamma$ points $\Gamma_0, \ldots, \Gamma_6$ in the hexagonal lattice for the NFE model. The parameters are $\Gamma M = 0.54$ Å$^{-1}$ and $\Gamma K = 0.62$ Å$^{-1}$. ($b$) Fragment of the energy spectrum of the 2D electron gas at the Bi/Si(111) surface in the NFE model corresponding to the bulk band gap (marked by $E_F$ in the left part of the figure) of around 0.2 eV between the bands where the Fermi level is located, creating the possibility of the edge state existence within this gap, and making the system a possible new topological insulator

0.6–1.1 eV $\cdot$ Å for $\alpha_R$. The structure of reciprocal space vectors connecting the equivalent $\Gamma$ points $\Gamma_0, \ldots, \Gamma_6$ in the hexagonal lattice is shown in Fig. 1 $a$. In the model originally proposed in [46], only the vectors $\mathbf{G}_1$, $\mathbf{G}_2$, $\mathbf{G}_6$ were included in order to describe states near the $M$ point, and we later expanded this model [47] with vectors $\mathbf{G}_3$, $\mathbf{G}_4$, $\mathbf{G}_5$ for the description of states in the entire BZ. The parameters of the hexagonal lattice in Fig. 1$a$ are $\Gamma M = 0.54$ Å$^{-1}$ and $\Gamma K = 0.62$ Å$^{-1}$.

A Bloch eigenstate of the Hamiltonian $H = H_0 + V$ is a two-component spinor that can be constructed in the NFE approximation in the form

$$\Psi_{\mathbf{k}}^{bulk}(\mathbf{r}) = \sum_n a_{n\mathbf{k}} \psi_{n\mathbf{k}}^{bulk}(\mathbf{r}) \tag{3}$$

where the Rashba eigenstates $\psi_{n\mathbf{k}}^{bulk} = \psi_{\mathbf{k}+\mathbf{G}_\mathbf{n}}^{bulk}$ have the form of free electron states with the quasimomentum shifted by the vector $\mathbf{G}_\mathbf{n}$ (see Fig. 1$a$) and

$$\psi_{\mathbf{k}}^{bulk} = \frac{e^{i\mathbf{k}\cdot\mathbf{r}}}{\sqrt{2}} \begin{pmatrix} 1 \\ \pm \exp\left[i\mathrm{Arg}(k_y - ik_x)\right] \end{pmatrix}. \quad (4)$$

The "±" sign corresponds to two eigenvalues for the Rashba energy spectrum $E(k) = \hbar^2 k^2/2m \pm \alpha_R k$.

In Fig. 1*b*, we plot a fragment of the energy spectrum of the 2D electron gas at the Bi/Si(111) surface in the NFE model corresponding to the bulk band gap (marked by $E_F$ at the left part of the figure) of around 0.2 eV between the bands where the Fermi level is located, reported to be above the second spin-split band [46]. The Fermi level position in the bulk gap, where the gapped structure of the electron spectrum is produced by the hexagonal lattice with potential (2), creates the possibility of edge state formation with energies in this gap, and, as we see below, makes the system a possible new candidate to the topological insulator class. The large metallic-like values of the electron energy and SOC amplitude present for the 2D electron gas in this system make it promising for the consideration in transport and optical experiments where the disorder, collision, and thermal broadening prevents the application of conventional semiconductors. We note that the discussed properties of the band structure for the Bi/Si 2D electron gas are obtained in the framework of one specific model with a set of parameters chosen for the best fit to experimental data. Hence, it may be modified in the future when more insight is gained into the properties of Bi/Si or other similar compounds. Still, we see below that the qualitative and topologically described features of the electron states studied within this model are robust against significant variations of the model parameters, which is an indication of certain intrinsic and stable properties of the system.

### 2.2. Edge states

We now turn our attention to the construction of the model for edge states localized at the opposite edges of a finite strip formed in the 2D electron gas. We can start with the strip geometry where the electrons are confined along the $y$ direction in the strip $-L/2 \le y \le L/2$ and with the conventional assumption of the hard-wall boundary conditions $\Psi(x, y = \pm L/2) = 0$ [8–10, 35, 36].

First, the spectrum of edge states can be found by solving the eigenstate problem with the requirement of an exponential dependence across the strip direction $y$. This can be done by starting from the bulk Hamiltonian and replacing the quasimomentum component in the direction of confinement by the purely imaginary variable describing the inverse localization depth corresponding to the localized states $\exp(\pm\Lambda y)$, which in our case means the substitution $k_y \to -i\Lambda$. We note that $\Lambda$ can be complex in general, with the imaginary part corresponding to oscillations of the edge wavefunctions on top of the exponential decay [8, 35], while in other models [9], $\Lambda$ is taken purely real, as in our system. The reason for a purely real $\Lambda$ in our model of edge states is the narrow bulk gap formed in the bulk spectrum originating from Hamiltonian (1) with the strong Rashba SOC. If we add more real nonzero wavevector components by adding the imaginary part to $\Lambda$, then the resulting energy increase pushes the edge states out of the bulk gap, making them unsuitable for the TI phase.

The eigenfunctions of this Hamiltonian can be constructed in the same nearly free-electron approximation as bulk states (3), and have the form

$$\Phi_{k_x\Lambda}(x, y) = e^{\Lambda y} F_{k_x\Lambda}(x), \quad (5)$$

$$F_{k_x\Lambda}(x) = \sum_n a_n(k_x, \Lambda)\phi_{nk_x\Lambda}(x). \quad (6)$$

The spinors $\phi_{nk_x\Lambda}(x)$ can be obtained from (4) by the substitution $k_y \to -i\Lambda$, which results in a purely imaginary number under the Arg function, giving

$$\phi_{nk_x\Lambda}(x) = \frac{\exp\left[i(k_x + nG)x\right]}{\sqrt{2}} \times \times \begin{pmatrix} 1 \\ \mp i\,\mathrm{sign}(k_x + nG + \Lambda) \end{pmatrix}. \quad (7)$$

The summation in (6) is over the 1D lattice in the reciprocal space, corresponding not to the 2D hexagonal but the 1D simple lattice along the $x$ direction formed by the vectors $\mathbf{G}_1$ and $\mathbf{G}_4$ in Fig. 1*a*, with the real space period $a = 2\pi/G$, where $G = 1.08\,\text{Å}^{-1}$ is the length of the $\mathbf{G}_i$ vector. State (6) remains a Bloch function along $x$ with the conventional translation property

$$\Phi_{k_x\Lambda}(x + a, y) = \exp(ik_x a)\Phi_{k_x\Lambda}(x, y),$$

while along the confinement direction, the wavefunctions are exponentials $\exp(\pm\Lambda y)$. If we solve the Schrödinger equation for our model of the 2D electron gas at the Bi/Si interface with the substitution $k_y \to -i\Lambda$ (without considering the specific boundary conditions at this stage), then the spectrum of edge states is obtained as a function of two parameters $(k_x, \Lambda)$. If there are eigenstates with energies corresponding to the gap in the bulk spectrum, they can be interesting as potential candidates for the edge states with topological protection.

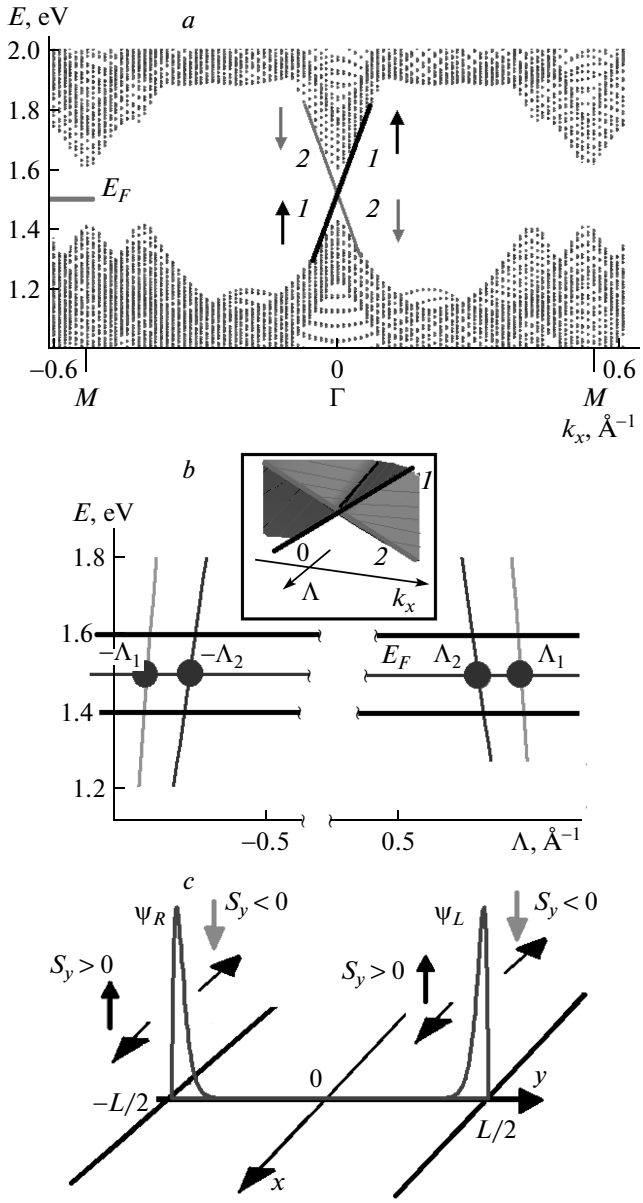


**Fig. 2**

The wavefunction satisfying the boundary conditions $\Psi_{k_x}(x, y = \pm L/2) = 0$ on a single edge and having the specific energy $E = E(k_x, \Lambda)$ in the bulk gap has the form of a linear combination of (6) with different localization lengths $\Lambda_{1,2}$ corresponding to the given energy $E = E(k_x, \Lambda_{1,2})$:

$$\Psi_{k_x}(x, y) = \sum_{\Lambda} c_\Lambda \Phi_{k_x \Lambda}(x, y). \qquad (8)$$

If the edge is represented by another and more smoothly increasing potential differing from the hard wall, or a more sophisticated boundary condition is chosen, the edge wavefunction is expected to be modified mainly in a small vicinity of the edge where a decaying tail can be formed. Because this modification would not strongly affect the global shape of the edge state and the main localization parameter, as well as the primary property of their possible topological stability induced by the presence of the topological invariant for the bulk states, we proceed with the simple hard-wall condition introduced above. We have found that in our model, the edge states indeed exist in the gap of the bulk spectrum. Their dependence on the $k_x$ parameter is shown in Fig. 2*a* as two linear dispersion curves *1* and *2* crossing the bulk gap for a typical value of the inverse localization length $\Lambda = 0.6$ Å$^{-1}$, together with the bulk spectrum plotted as a function of $k_x$ for all values of $k_y$ in the 2D BZ shown in Fig. 1*a*. The joint dependence of the energy of edge states on both $k_x$ and $\Lambda$ is shown as a 3D plot in the inset to Fig. 2*b*. The two spin-resolved energy branches $E = E(k_x, \Lambda)$ are shaded differently (branch *1* is dark gray and branch *2* is light gray) depending on their spin projection $S_y$. In Fig. 2*a*, we also plot the mean values of the only nonvanishing spin component $S_y = \langle\Psi|\sigma_y|\Psi\rangle$ for the edge states that are coupled to their direction of mo-

**Fig. 2.** (*a*) Bulk (grayscale dots on the background) and edge (black and gray linear dispersions marked as *1* and *2*) energy bands in a Bi/Si strip shown as a function of $k_x$ for all $k_y$ (bulk states) and for the typical value of the inverse localization length $\Lambda = 0.6$ Å$^{-1}$ (for edge states). The edge states are formed in the bulk energy gap where the Fermi level position is shown, and have the opposite spin polarization coupled to their group velocity for left-moving electrons (band *2*) and right-moving electrons (band *1*). (*b*) The edge-state energy dependence on the inverse localization length parameter $\Lambda$ taken for $k_x = 0.05$ Å$^{-1}$. For a given position of the Fermi level in the bulk gap, there are two roots $\pm\Lambda_{1,2}$ for each edge of the strip yielding two edge wavefunctions belonging to the corresponding branches of the energy spectrum. The inset shows the side view of the edge state spectrum as a function of both $k_x$ and $\Lambda$, demonstrating the 3D structure of two branches *1* and *2* of spin split states intersecting along the line $k_x = 0$. (*c*) Edge states localized on the opposite borders of the strip for the edge-state energy equal to the Fermi level inside the bulk gap, $E_F = 1.5$ eV, and for the strip width $L = 10$ nm. The edge states are well localized at the corresponding edge of the strip. For each edge, there are two states propagating to the positive and negative directions of the $x$ axis and having opposite spin polarizations $S_y$

tion along the strip. The spin-up states move to the right with the group velocity

$$v_x = \hbar^{-1}\partial\varepsilon/\partial k_x > 0,$$

while the spin-down states move to the left ($v_x < 0$), shown in the same gray-scale level with the corresponding branches of the edge spectrum.

An important feature of the edge state spectrum is the presence of two roots $\Lambda_{1,2}$ for each energy value for a given $k_x$; the equation $E(k_x, \Lambda) = E_0$ has two pairs of solutions $\pm\Lambda_{1,2}$ for the left and right edge of the strip, as is shown in Fig. 2*b* for the dependence of the energy on $\Lambda$ at $k_x = 0.05\,\text{Å}^{-1}$. Such a structure of energy eigenvalues is a direct consequence of the relative proximity of two branches of the Rashba spectrum present in the basis for the Hamiltonian, which can be also seen for the bulk spectrum in Fig. 1*b*. This feature allows constructing the edge states satisfying the boundary conditions for a band of energies located in the bulk energy gap, as is done in various models of edge states in TIs [8, 9, 35, 36].

The specific boundary conditions are applied to the general form of the edge state in Eq. (8). The two wavefunctions for a given energy $E = E(k_x, \Lambda_{1,2})$ satisfying the boundary condition $\Psi_L(x, y = L/2) = 0$ on the left edge of the strip $y = L/2$ (in the forward direction of the $x$ axis) and decaying into the strip have form (8) and can be constructed explicitly by the following superposition of states (6):

$$\Psi_L^{(1)}(x,y) = F_{k_x\Lambda_1}(x) \times \times \left\{\exp(\Lambda_1 y) - \exp\left[(\Lambda_1 - \Lambda_2)\frac{L}{2} + \Lambda_2 y\right]\right\}, \quad (9)$$

$$\Psi_L^{(2)}(x,y) = F_{k_x\Lambda_2}(x) \times \times \left\{\exp(\Lambda_2 y) - \exp\left[(\Lambda_2 - \Lambda_1)\frac{L}{2} + \Lambda_1 y\right]\right\}, \quad (10)$$

where the normalization condition is implied in $F_{k_x\Lambda}(x)$. Accordingly, the localized wavefunctions for the right edge $y = -L/2$ can be written as

$$\Psi_R^{(1)}(x,y) = F_{k_x-\Lambda_1}(x) \times \times \left\{\exp(-\Lambda_1 y) - \exp\left[(\Lambda_1 - \Lambda_2)\frac{L}{2} - \Lambda_2 y\right]\right\}, \quad (11)$$

$$\Psi_R^{(2)}(x,y) = F_{k_x-\Lambda_2}(x) \times \times \left\{\exp(-\Lambda_2 y) - \exp\left[(\Lambda_2 - \Lambda_1)\frac{L}{2} - \Lambda_1 y\right]\right\}. \quad (12)$$

All the edge states in (9), (10) and (11), (12) have different spinor parts $F_{k_x\pm\Lambda_{1,2}}$ due to the different value of parameter $\pm\Lambda_{1,2}$, and in general may describe different spin polarization. We note that their spin properties are described by the mean value of spin calculated for the edge state that is not itself labeled by the spin quantum number, which is typical in the systems with SOC where the spin operator does not commute with the Hamiltonian. Still, because the direction of propagation of 1D edge states is strongly coupled to the sign of the mean spin polarization and the edge subband index, we can link these two properties together and describe the edge states as having a definite mean spin value.

An example of edge wavefunctions is shown in Fig. 2*c* for the energy of the edge state equal to the Fermi level inside the bulk gap, $E = E_F = 1.5$ eV, and for the strip width $L = 10$ nm. We can see that the edge states are well localized at the corresponding edge of the strip on the length of about 1 nm, which may lead to the formation of topologically protected edge modes if the corresponding bulk topological invariant is nontrivial, as is discussed in the next section. The arrows indicate the direction of propagation and the spin $S_y$ of each state in pair (9), (10) and (11), (12). The direction of the propagation of two chiral states on one edge $y = -L/2$ in our model is the same as on the other edge $y = L/2$, which can be explained by the strong Rashba SOC in our system, leading, among other things, to the dominant polarization $S_y$ of the states moving in the $x$ direction. Here, the noncompensated total spin $S_y$ can be accumulated if the population of right-moving and left-moving electrons is unbalanced, for example, by an external electric field $E \parallel Ox$, as is the case in various models with current-induced spin polarization both in conventional materials with strong SOC and in TIs [72], which can also be expected for the edge states shown in Fig. 2*c*.

The form of spin polarization shown in Figs. 2*a* and 2*c* creates a positive expectation about their topological stability for charge transport against the scattering on nonmagnetic impurities that do not violate the time-reversal symmetry, if supported by the analysis of the topological properties of bulk states indicating the presence of a nontrivial topological invariant. If we consider backscattering, then it is clear from Fig. 2*c* that the change of the propagation direction would lead to spin flip, and this cancels the reflected waves and extinguishes the backscattering [1, 2]. This is consistent with the arguments of the topological stability of such edge states as the participants of charge transport, which is the required property of a system to become a TI.

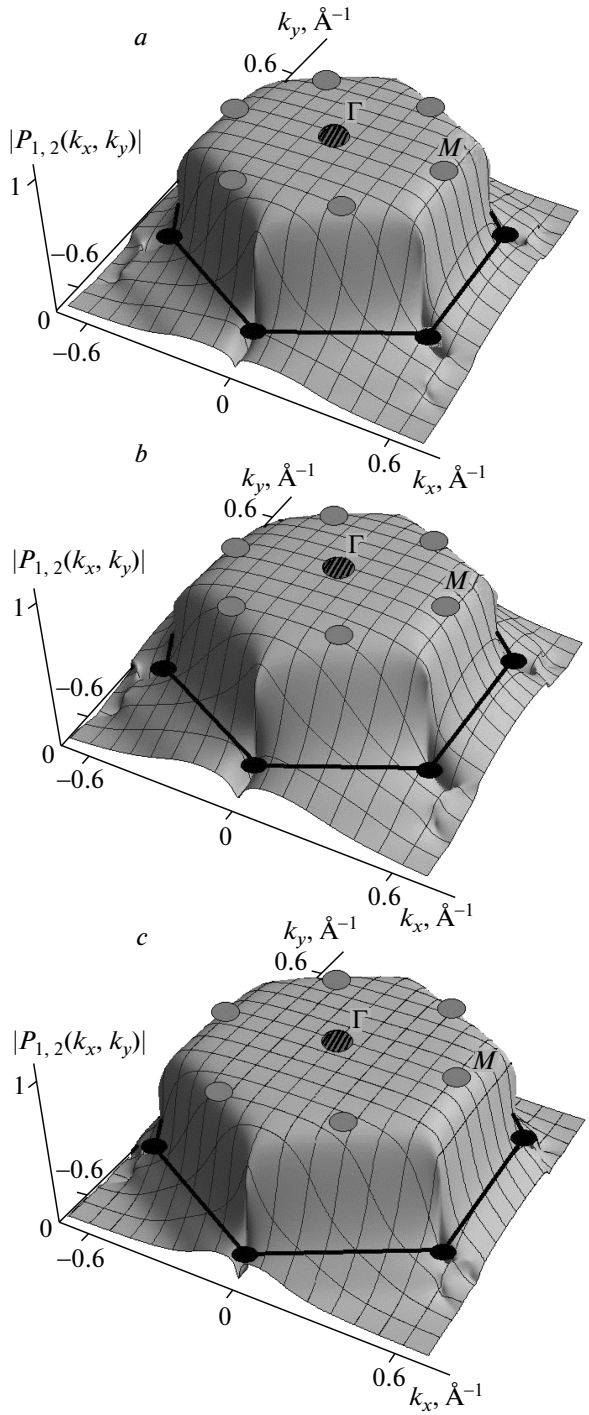


Fig. 3

We see in Sec. 3 below that our assumption about the 2D electron gas on the Bi/Si interface as a possible TI is supported further by the analysis of the topological properties of 2D bulk states.

## 3. TOPOLOGICAL PROPERTIES OF BULK STATES

It is known from the general theory that the stability of edge states is guaranteed by certain topological properties of bulk states. In particular, the system can be a TI if an integer called the $Z_2$ invariant is different from zero [1, 2, 6, 21]. There are several ways to calculate this invariant, and here we use the method proposed by Kane and Mele [6], which links the $Z_2$ index to the zeros of the Pfaffian for the interband matrix elements of the time-reversal operator between the occupied bands, which has the form $\Theta = i\sigma_y K$ for spin-1/2 particles, where $K$ is the complex conjugation operator. If we have only two lowest bands occupied, which is the case of the 2D electron gas in Bi/Si 2DEG, then the Pfaffian $P_{1,2}(\mathbf{k})$ is equal to the single off-diagonal matrix element between the Bloch functions $u_{1,2}(\mathbf{k})$ in the occupied bands 1 and 2,

$$P_{1,2}(\mathbf{k}) = \langle u_1(\mathbf{k})|\Theta|u_2(\mathbf{k})\rangle. \qquad (13)$$

The topological considerations provide a convenient form of using definition (13) for the finding new materials demonstrating TI properties. If, for a hexagonal BZ, the $\mathbf{k}$-dependent function $P(\mathbf{k})$ has pairs of zeros in the corners of the BZ (or, depending on the overall symmetry, on the lines inside the BZ), then the system demonstrates the properties of a TI [6, 11, 21]. There is an extensive discussion of the $Z_2$ invariant properties related to TIs including another definition of this invariant, where the matrix elements of the TR operator $\Theta$ are calculated between the states with opposite wavevectors $\mathbf{k}$ and $-\mathbf{k}$ and the TI is determined by its properties not in the entire BZ but at a discrete set of "time reversal invariant points" like the $\Gamma$ or $M$ points. The detailed discussion and all relevant mathematical connections between different approaches to the calculation of the $Z_2$ invariant can be found in the literature [1, 2, 21, 23, 30, 73–75].

**Fig. 3.** The absolute value of Pfaffian (13) in the hexagonal BZ for the 2D electron gas on the Bi/Si interface for different values of bulk band parameters: ($a$) $V_0 = 0.3$ eV, $\alpha_R = 1.1$ eV · Å; ($b$) $V_0 = 0.6$ eV, $\alpha_R = 1.1$ eV · Å; and ($c$) $V_0 = 0.3$ eV, $\alpha_R = 0.6$ eV · Å. The Pfaffian has three pairs of zeros at the corners of the BZ, where the visible zeros are shown as black circles while at TR-invariant $\Gamma$ and $M$ points shown as shaded and gray circles, the value is $|P_{1,2}| = 1$. These properties indicate that the $Z_2$ invariant is odd, and the topological insulator phase is present for all three sets of material parameters

In Fig. 3*a*, we plot the absolute value of Pfaffian (13) in the hexagonal BZ for the 2D electron gas on the Bi/Si interface for the same basic set of model parameters as were used for calculations of the bulk spectrum in Fig. 1*b*. To see the possible changes in the $Z_2$ index with the variation of the system parameters, we plot $|P_{1,2}|$ for two other sets of parameters: in Fig. 3*b*, the amplitude of the periodic potential is increased compared to the basic case shown in Fig. 1*b*, $V_0 = 0.6$ eV, and the Rashba SOC amplitude is the same, $\alpha_R = 1.1$ eV $\cdot$ Å; in Fig. 3*c*, the periodic potential amplitude is the same as in Fig. 3*a*, $V_0 = 0.3$ eV, but the Rashba coupling amplitude is decreased, $\alpha_R = 0.6$eV $\cdot$ Å. It is clearly seen for all cases that the Pfaffian has zeros in the corners of the BZ, where the visible zeros are shown as black circles whose border is shown schematically, while $|P_{1,2}| = 1$ at the TR-invariant $\Gamma$ and $M$ points, respectively shown as shaded and dark gray circles. There are three pairs of zeros for $|P_{1,2}|$, which indicates that the $Z_2$ invariant is odd, thus classifying the 2D electron gas on the Bi/Si interface as a TI with protected edge states [1, 2, 6, 21]. The presentation of the structure of the Pfaffian in Fig. 3 in the whole BZ is useful in determining the areas where the states of different bands belong to the "even" or "odd" subspace relative to the action of the time reversal operator $\Theta$, in accordance with the classification proposed by Kane and Mele [6]. In our case shown in Fig. 3, we see that the major part of the BZ corresponds to the states belonging to the even subspace with $|P(\mathbf{k})| = 1$; however, in approaching the borders of the BZ, the value of $|P(\mathbf{k})|$ is modified significantly, and in the corners we obtain the odd subspace where $|P(\mathbf{k})| = 0$, and therefore the TI property is present.

We can also see in Fig. 3 that the variations of material parameters do not significantly change the topological properties of the Pfaffians, which all have the same qualitative features with $|P_{1,2}| = 1$ at the time-reversal-invariant $\Gamma$ and $M$ points and with three pairs of zeros for $|P_{1,2}|$ in the corners of the BZ. The depth of the parameter variation present in three parts of Fig. 3 is rather big and reaches 50 %, which covers a wide range of possible experimental and technological fabrication of the 2D electron gas on the Bi/Si interface. Still, the absolute values of the Pfaffians shown in Fig. 3 look very similar to each other, indicating their qualitative topological nature, which is the key for discovering new examples of TIs. The method of mutual analysis of chiral edge states and topological bulk properties used in our calculations can be applied to other materials and structures.

## 4. CONCLUSIONS

We have derived a model for the one-dimensional edge states for the electrons on the bismuth on silicon interface in a finite strip geometry. Based on the bulk nearly free-electron model, their energy dispersion was obtained inside the bulk gap, to be linear in the quasimomentum. The spin polarization of edge states is related to the direction of propagation along the given edge, which provides topological stability of these chiral modes. The topological stability of edge states was confirmed by the structure of the interband matrix element for the time reversal operator, which was shown to be stable against large variations of the material parameters. The results in this paper may be of interest both for the development of the topological insulator theory by providing a novel example of the material belonging to this class, and for the development of new spintronics and nanoelectronics devices with stable transport and operating at room temperature.

The authors are grateful to V. Ya. Demikhovskii, A. M. Satanin, A. P. Protogenov, G. M. Maximova, V. A. Burdov, and A. A. Konakov for the helpful discussions. The work is supported by the RFBR (grants Nos. 13-02-00717a, 13-02-00784a).

## REFERENCES

1. M. Z. Hasan and C. L. Kane, Rev. Mod. Phys. **82**, 3045 (2010).

2. X.-L. Qi and S.-C. Zhang, Rev. Mod. Phys. **83**, 1057 (2011).

3. J. E. Moore, Nature **464**, 194 (2010).

4. D. Culcer, Physica E **44**, 860 (2012).

5. X.-L. Qi, T. L. Hughes, and S.-C. Zhang, Phys. Rev. B **78**, 195424 (2008).

6. C. L. Kane and E. J. Mele, Phys. Rev. Lett. **95**, 146802 (2005); **95**, 226801 (2005).

7. B. A. Bernevig, T. L. Hughes, and S.-C. Zhang, Science **314**, 1757 (2006).

8. M. König, H. Buhmann, L. W. Molenkamp, T. L. Hughes, C.-X. Liu, X.-L. Qi, and S-C. Zhang, J. Phys. Soc. Jpn. **77**, 031007 (2008).

9. B. Zhou, H.-Z. Lu, R.-L. Chu, S.-Q. Shen, and Q. Niu, Phys. Rev. Lett. **101**, 246807 (2008).

**10**. V. Krueckl and K. Richter, Phys. Rev. Lett. **107**, 086803 (2011).

**11**. S. Murakami, Phys. Rev. Lett. **97**, 236805 (2006); M. Wada, S. Murakami, F. Freimuth, and G. Bihlmayer, Phys. Rev. B **83**, 121310 (R) (2011).

**12**. T. E. Huber, A. Adeyeye, A. Nikolaeva et al., Phys. Rev. B **83**, 235414 (2011).

**13**. J. G. Rodrigo, A. García-Martín, J. J. Sáenz, and S. Vieira, Phys. Rev. Lett. **88**, 246801 (2002); C. Sabater, D. Gosálbez-Martínez, J. Fernández-Rossier et al., arXiv:1304.0934 (2013).

**14**. H.-J. Zhang, S. Chadov, L. Müchler et al., Phys. Rev. Lett. **106**, 156402 (2011).

**15**. X.-L. Qi, Y.-S. Wu, and S.-C. Zhang, Phys. Rev. B **74**, 085308 (2006).

**16**. M. Ezawa, Phys. Rev. Lett. **109**, 055502 (2012); Phys. Rev. B **86**, 161407 (2012); Phys. Rev. Lett. **110**, 026603 (2013); arXiv:1303.1245 (2013).

**17**. N. D. Drummond, V. Zólyomi, and V. I. Fal'ko, Phys. Rev. B **85**, 075423 (2012).

**18**. A. A. Burkov, M. D. Hook, and L. Balents, Phys. Rev. B **84**, 235126 (2011).

**19**. C. Liu, T. L. Hughes, X.-L. Qi et al., Phys. Rev. Lett. **100**, 236601 (2008).

**20**. I. Knez, R.-R. Du, and G. Sullivan, Phys. Rev. Lett. **107**, 136603 (2011).

**21**. L. Fu and C. L. Kane, Phys. Rev. B **74**, 195312 (2006); Phys. Rev. B **76**, 045302 (2007).

**22**. L. Fu, C. L. Kane, and E. J. Mele, Phys. Rev. Lett. **98**, 106803 (2007).

**23**. T. Fukui and Y. Hatsugai, Phys. Rev. B **75**, 121403(R) (2007).

**24**. L. Fu, Phys. Rev. Lett. **106**, 106802 (2011).

**25**. J.-M. Hou, W.-X. Zhang, and G.-X. Wang, Phys. Rev. B **84**, 075105 (2011).

**26**. M. Levin, F. J. Burnell, M. Koch-Janusz, and A. Stern, Phys. Rev. B **84**, 235145 (2011).

**27**. Y. Li, X. Zhou, and C. Wu, Phys. Rev. B **85**, 125122 (2012).

**28**. R.-J. Slager, A. Meszaros, V. Juričič, and J. Zaanen, Nature Phys. **9**, 98 (2013).

**29**. B. Douçot, M. V. Feigel'man, L. B. Ioffe, and A. S. Ioselevich, Phys. Rev. B **71**, 024505 (2005).

**30**. A. P. Schnyder, S. Ryu, A. Furusaki, and A. W. W. Ludwig, Phys. Rev. B **78**, 195125 (2008).

**31**. A. D. Mirlin, F. Evers, I. V. Gornyi, and P. M. Ostrovsky, Int. J. Mod. Phys. B **24**, 1577 (2010).

**32**. D. Hsieh, D. Qian, L. Wray et al., Nature (London) **452**, 970 (2008).

**33**. K. Miyamoto, A. Kimura, T. Okuda et al., Phys. Rev. Lett. **109**, 166802 (2012).

**34**. I. A. Nechaev, R. C. Hatch, M. Bianchi et al., Phys. Rev. B **87**, 121111 (2013).

**35**. J. Linder, T. Yokoyama, and A. Sudbø, Phys. Rev. B **80**, 205401 (2009).

**36**. H.-Z. Lu, W.-Y. Shan, W. Yao et al., Phys. Rev. B **81**, 115407 (2010).

**37**. D. N. Sheng, Z. Y. Weng, L. Sheng, and F. D. M. Haldane, Phys. Rev. Lett. **97**, 036808 (2006).

**38**. S. Caprara, V. V. Tugushev, P. M. Echenique, and E. V. Chulkov, Phys. Rev. B **85**, 121304(R) (2012).

**39**. S.-T. Lee, S.-M. Huang, and C.-Y. Mou, arXiv: 1308.4053 (2013).

**40**. T. Hirahara, T. Nagao, I. Matsuda et al., Phys. Rev. Lett. **97**, 146803 (2006).

**41**. T. Hirahara, T. Nagao, I. Matsuda et al., Phys. Rev. B **75**, 035422 (2007).

**42**. E. Frantzeskakis, S. Pons, H. Mirhosseini et al., Phys. Rev. Lett. **101**, 196805 (2008).

**43**. J. H. Dil, F. Meier, J. Lobo-Checa et al., Phys. Rev. Lett. **101**, 266802 (2008).

**44**. I. Gierz, T. Suzuki, E. Frantzeskakis et al., Phys. Rev. Lett. **103**, 046803 (2009).

**45**. J. Ibañez-Azpiroz, A. Eiguren, and A. Bergara, Phys. Rev. B **84**, 125435 (2011).

**46**. E. Frantzeskakis, S. Pons, and M. Grioni, Phys. Rev. B **82**, 085440 (2010).

**47**. D. V. Khomitsky, Zh. Eksp. Teor. Fiz. **141**, 848 (2012).

**48**. T. Hirahara, K. Miyamoto, I. Matsuda et al., Phys. Rev. B **76**, 153305 (2007).

**49**. G. Bian, T. Miller, and T.-C. Chiang, Phys. Rev. B **80**, 245407 (2009).

**50**. K. Sakamoto, H. Kakuta, K. Sugawara et al., Phys. Rev. Lett. **103**, 156801 (2009).

**51**. D. N. Sheng and Z. Y. Weng, Phys. Rev. B **54**, R11070 (1996).

**52**. A. Ström, H. Johannesson, and G. I. Japaridze, Phys. Rev. Lett. **104**, 256804 (2010).

**53**. S. Basak, H. Lin, L. A. Wray et al., Phys. Rev. B **84**, 121401(R) (2011).

**54**. D. Niesner, Th. Fauster, S. V. Eremeev et al., Phys. Rev. B **86**, 205403 (2012).

**55**. S. V. Eremeev, I. V. Silkin, T. V. Menshchikova, A. P. Protogenov, and E. V. Chulkov, Pis'ma v Zh. Eksp. Teor. Fiz. **96**, 870 (2012).

**56**. H.-J. Zhang, C.-X. Liu, X.-L. Qi et al., Phys. Rev. B **80**, 085307 (2009).

**57**. G.-W. Chern, Phys. Rev. B **81**, 125134 (2010).

**58**. A. Rüegg and G. A. Fiete, Phys. Rev. Lett. **108**, 046401 (2012).

**59**. D. Bercioux, N. Goldman, and D. F. Urban, Phys. Rev. A **83**, 023609 (2011).

**60**. J. D. Sau, R. Sensarma, S. Powell et al., Phys. Rev. B **83**, 140510(R) (2011).

**61**. A. Dyrdał and J. Barnaś, Phys. Rev. B **86**, 161401 (2012).

**62**. M. Dzero, K. Sun, P. Coleman, and V. Galitski, Phys. Rev. B **85**, 045130 (2012); Z.-Q. Huang, F.-C. Chuang, C.-H. Hsu et al., Phys. Rev. B **88**, 165301 (2013).

**63**. L. Craco and S. Leoni, Phys. Rev. B **85**, 195124 (2012).

**64**. R. H. Miwa, T. M. Schmidt, and P. Venezuela, Phys. Rev. B **72**, 125403 (2005).

**65**. K. Yaji, Y. Ohtsubo, S. Hatta et al., Nature Comm. 1:17 doi:10.1038/ncomms1016 (2010).

**66**. J. Ibañez-Azpiroz, A. Eiguren, E. Ya. Sherman, and A. Bergara, Phys. Rev. Lett. **109**, 156401 (2012).

**67**. K. Okamoto, K. Kuroda, H. Miyahara et al., Phys. Rev. B **86**, 195304 (2012).

**68**. K. Ishizaka, M. S. Bahramy, H. Murakawa et al., Nature Mater. **10**, 521 (2011).

**69**. V. Gnezdilov, D. Wulferding, P. Lemmens et al., arXiv:1303.4333 (2013).

**70**. S. V. Eremeev, I. A. Nechaev, Yu. M. Koroteev et al., Phys. Rev. Lett. **108**, 246802 (2012); G. Landolt, S. V. Eremeev, Yu. M. Koroteev et al., Phys. Rev. Lett. **109**, 116403 (2012); S. V. Eremeev, I. A. Nechaev, and E. V. Chulkov, Pis'ma v Zh. Eksp. Teor. Fiz. **96**, 484 (2012); I. P. Rusinov, I. A. Nechaev, S. V. Eremeev et al., arXiv:1303.4987 (2013).

**71**. B. Rasche, A. Isaeva, M. Ruck et al., Nature Materials, doi:10.1038/nmat3570 (2013).

**72**. P. Kleinert, V. V. Bryksin, and O. Bleibaum, Phys. Rev. B **72**, 195311 (2005); V. V. Bryksin and P. Kleinert, Phys. Rev. B **73**, 165313 (2006); J. Wang, K. S. Chan, and D. Y. Xing, Phys. Rev. B **73**, 033316 (2006); J. Li and S.-Q. Shen, Phys. Rev. B **76**, 153302 (2007); D. V. Khomitsky, Phys. Rev. B **79**, 205401 (2009); Ph. Jacquod, Nanotechnology **21**, 274006 (2010); P. Bokes and F. Horváth, Phys. Rev. B **81**, 125302 (2010); P. Schwab, R. Raimondi, and C. Gorini, Europhys. Lett. **93**, 67004 (2011); D. Culcer, Phys. Rev. B **84**, 235411 (2011).

**73**. S. Ryu, C. Mudry, H. Obuse, and A. Furusaki, Phys. Rev. Lett. **99**, 116601 (2007).

**74**. R. Roy, Phys. Rev. B **79**, 195321 (2009).

**75**. R. Yu, X. L. Qi, A. Bernevig et al., Phys. Rev. B **84**, 075119 (2011).